

The effect of boron amount in the electrolyte on the corrosion properties of Ti45Nb coated by PEO

Elektrolit içerisindeki bor miktarının PEO ile kaplanan Ti45Nb'nin korozyon özelliklerine etkisi

S. Yenal VANGÖLÜ^{1,2,*}, Özgü BAYRAK³

¹Atatürk Üniversitesi, Metalürji ve Malzeme Mühendisliği Bölümü, Erzurum, Türkiye

²University of Leeds, Institute of Functional Surfaces (IFS), Leeds, UK

³Bakırçay Üniversitesi, Biyomedikal Mühendisliği Bölümü, İzmir, Türkiye

• Received: 07.08.2023

• Accepted: 29.09.2023

Abstract

Developing more biocompatible biomaterials with mechanical properties similar to those of cortical bone has long been a challenge for scientists. They are still working on new alloys and coating processes to meet this challenge. Among these biocompatible materials, β -titanium alloys, which will prevent stress-shielding and have a Poisson's ratio very close to the cortical bone, have been attracting the attention of scientists for a long time. In addition to this, the PEO method, which makes it possible to embed ions into the oxide layer, has also come to the fore in recent years as a surface treatment in order to increase the corrosion resistance, wear resistance and biocompatibility of biomaterials and also to provide antibacterial/antimicrobial properties. In this study, Ca and P-containing oxide layers with two different boron content and no boron content were successfully formed on Ti45Nb β -titanium alloy substrate by using the PEO method. Surface characterization and corrosion resistance tests of these layers were carried out. The obtained results were compared with each other and with the uncoated substrate. XRD analysis showed that the coatings are primarily composed of two major polymorphs of TiO_2 , anatase and rutile. Static electrochemical measurements were made in diluted Foetal Bovine Serum (FBS) and hydrogen peroxide added serum. H_2O_2 was added to simulate the inflammatory state in the body. The measurements showed that all the coated samples had lower corrosion current densities compared to the uncoated ones both in serum and H_2O_2 -added serum.

Keywords: Boron, Corrosion, PEO, Ti45Nb

Öz

Kortikal kemiğe benzer mekanik özelliklere sahip daha biyouyumlu biyomalzemeler geliştirmek uzun zamandır bilim adamları için bir zorluk olmuştur. Bu zorluğun üstesinden gelmek için hala yeni alaşımlar ve kaplama süreçleri üzerinde çalışmalar sürmektedir. Bu biyouyumlu malzemeler arasında stres kalkanı etkisini önleyecek ve kortikal kemiğe çok yakın Poisson oranına sahip β -titanyum alaşımları uzun süredir bilim insanlarının ilgisini çekmektedir. Bunun yanı sıra oksit tabakasına iyon gömmeyi mümkün kılan PEO yöntemi, biyomalzemelerin korozyon direncini, aşınma direncini ve biyouyumluluğunu artırmak aynı zamanda antibakteriyel/antimikrobiyal özellikler sağlamak amacıyla son yıllarda bir yüzey işlemi olarak öne çıkmaktadır. Bu çalışmada, PEO yöntemi kullanılarak Ti45Nb β -titanyum alaşımlı altlık üzerinde iki farklı bor içeriğine sahip ve bir de bor içermeyen Ca ve P içeren oksit tabakaları başarıyla oluşturulmuştur. Bu tabakaların yüzey karakterizasyonları ve korozyon dayanım testleri yapılmıştır. Elde edilen sonuçlar kendi aralarında ve kaplanmamış numuneler ile karşılaştırılmıştır. XRD analizlerinde kaplamaların temel olarak iki ana TiO_2 polimorfundan, anataz ve rutilden oluştuğu görülmüştür. Seyreltilmiş Fetal Sığır Serumuna (FBS) ve hidrojen peroksit eklenmiş serumda statik elektrokimyasal ölçümler yapılmıştır. H_2O_2 vücuttaki enflamatuar durumu simüle etmek için eklenmiştir. Ölçümler, kaplanmış tüm numunelerin hem serumda hem de H_2O_2 ilaveli serumda kaplanmamış olanlara kıyasla daha düşük korozyon akımı yoğunluklarına sahip olduğunu göstermiştir.

Keywords: Bor, Korozyon, PEO, Ti45Nb

*a S. Yenal Vangölü; yvangolu@atauni.edu.tr

1. Introduction

Nowadays a wide spectrum of materials, which are expected to exhibit specific properties, are used for biomedical applications. The most important properties required from a biomaterial can be said as biocompatibility and corrosion resistance in the order of importance (Elias et al., 2008; Gebert et al., 2016; Long & Rack, 1998; Niinomi, 2003). In terms of biocompatibility and corrosion resistance, titanium alloys are the most attractive among all of the known metallic biomaterials for biomedical applications such as artificial hip and knee joints, bone plates, pacemakers, fracture fixation screws, etc (Niinomi & Boehlert, 2015). Although commercial pure titanium and Ti6Al4V grades are the most widely used metallic biomaterials, the use of β -titanium alloys increased especially in the past two decades. One of the most important motives behind their development is to minimize the stress-shielding effect associated with the relatively high elasticity modulus of α and $\alpha+\beta$ titanium alloys as well as stainless steel and CoCr-based alloys (Chen & Thouas, 2014). A promising and relatively new β -Ti alloy Ti45Nb became prominent with its Young's moduli. The Young's modulus of Ti45Nb is significantly lower compared to both α and $\alpha+\beta$ titanium alloys and it is closer to that of the cortical bone, which reduces the stress-shielding effect commonly associated with other metallic implants (Bai et al., 2016; Ozaki et al., 2004; Valiev et al., 2015). Moreover, according to the scientific literature, it is a fact that Nb, which is known to be unreactive in the body and biocompatible, is beneficial for osteogenesis (Bai et al., 2016; Johansson & Albrektsson, 1991; Matsuno et al., 2001). This means that Ti45Nb implants can better distribute mechanical loads and promote improved bone remodelling and integration. Ti45Nb also has acceptable corrosion resistance, reducing the risk of metallic ion release into the biological system, which is of great importance in terms of ensuring the safety and long-term use of the implant in the body. Ti45Nb is a suitable material for a number of biomedical applications due to its great biocompatibility, advantageous mechanical qualities, and corrosion resistance. It is extensively utilised in the manufacture of orthopaedic implants including hip and knee joint replacements, bone plates, and fracture fixation screws. The aim of using Ti45Nb in biomedical applications is to enhance patient outcomes, mitigate risk and enhance the overall performance and lifespan of the implants.

Nowadays bone implants should acquire not only the above-mentioned features but also some additional properties. For example, it is expected for the new generation of bone implants to have some bioactive agents like growth factors, antibiotics, antibacterial agents, etc. on their surfaces (Yavari et al., 2016). As a result of the corrosion of metallic alloys, the metal ions and particles, which are potentially toxic, can be released into the biological system from the metallic implants (Esfahani et al., 2022). Even though Ti45Nb shows favourable mechanical and corrosion properties, it is expected from these implants in the biomaterials field to exhibit better or enhanced mechanical and corrosion properties in vivo. Surface modification of the implants stands out as one of the most common techniques that can be used to provide these desired properties. Surface modifications have been used as an effective way to form a film layer doped with desired agents and impart protection against the corrosion of metallic implants. Various surface modification techniques such as anodising, plasma spraying, ion implantation, PEO, etc. have been introduced to form such a thin-film layer.

The introduction of boron (B) or boron-doping into the surface of biomaterials has garnered significant interest in the field of biomaterials sciences. Boron, a trace element known to be antibacterial-antifungal, also enhances osseointegration and plays a vital role in bone formation. It is also biocompatible for certain doses (extremely high doses of boron (>20 mg in adults) can be toxic and even lethal). The bactericidal properties of boron make it an attractive option for fighting bacterial infections commonly associated with implantable devices. The research conducted by Sopchenski et al. (2018) revealed that when Cp-Ti samples were doped with a combination of calcium (Ca), phosphorus (P), and boron using PEO, the resulting TiO₂ layer exhibited significant bactericidal effects against *S. aureus* and *P. Aeruginosa*. According to some studies, boron leads to improved bone strength and stability as it promotes calcium mineralization and bone generation. Besides, when used in appropriate amounts, boron on the implant surface is considered to be safe and biocompatible and enhances dental stem cells and osteogenic differentiation, supporting the growth and differentiation of bone marrow stromal cells (Atila et al., 2016; Cheng et al., 2011; Hakki et al., 2010; Taşlı et al., 2013; Vangolu & Kilic, 2022; Ying et al., 2011).

Many researchers have used surface engineering in biomaterials since it was recognised that the surface properties of biomaterials affect the biological response of the host to the implants (Zorn et al., 2005). Surface modifications are now aimed at improving bioactivity, biocompatibility, wear and corrosion resistance, and bactericidal activity. Surface engineering techniques such as plasma spraying, ion implantation, and plasma

electrolytic oxidation have been used to dope biomaterial surfaces with bactericidal elements (boron, silver, copper, etc.) as well as biocompatible and bioactive elements (HA, CaP, etc.). PEO has risen to prominence among these approaches in recent years due to its benefits over other surface modification technologies.

PEO is considered to be a versatile and effective technique for NPs-doping and ionic-doping of elements and surface modification of biomaterials as it has many advantages such as improved coating adhesion, customizable surface properties, enhanced corrosion resistance, increased surface hardness, time and cost efficiency, environmental friendliness and compatibility with complex geometries. A high-voltage electrical discharge is applied to a biomaterial submerged in an electrolyte solution during the PEO process, resulting in a plasma micro-discharge on its surface. Bactericidal and/or bioactive ions or particles can be doped into the resultant oxide layer generated on the biomaterial surface by incorporating bactericidal or bioactive chemicals or particles into the electrolyte.

In this study, different amounts of boron-doped oxide layers were formed on Ti45Nb substrates. The corrosion resistance of these samples in serum and hydrogen peroxide-added serum. Hydrogen peroxide was added to the serum to create the infection conditions. The results were compared with the uncoated substrate. Porous and rough layers containing boron on Ti45Nb substrates were successfully formed using the PEO method.

2. Material and method

2.1. Materials

Commercial wrought Ti45Nb alloy (Grade 36) was used to produce $14 \times 14 \times 3$ mm³ samples. All surfaces were polished using SiC abrasive paper and diamond suspension to the maximum roughness of 80 nm. Then the substrates were cleaned using ethanol and distilled water prior to coating deposition. The electrolyte solution used in the PEO process has consisted of calcium acetate monohydrate ($\text{Ca}(\text{C}_2\text{H}_3\text{O}_2)_2 \cdot \text{H}_2\text{O}$ - Merck), trisodium phosphate dodecahydrate ($\text{Na}_3\text{PO}_4 \cdot 12\text{H}_2\text{O}$ - Merck), disodium tetraborate decahydrate ($\text{Na}_2\text{B}_4\text{O}_7 \cdot 10\text{H}_2\text{O}$ - Merck) and distilled water. The amounts of calcium acetate hydrate and tri-Sodium phosphate dodecahydrate were kept constant while the amount of di-Sodium tetraborate decahydrate was changed in order to evaluate the effect of boron on the coatings. The reagents and the amounts used to prepare the electrolytes for 1000 ml were determined based on our previous studies (Vangolu & Kilic, 2022) and scientific literature (Sopchenski et al., 2018) and are given in Table 1.

Table 1. The reagents and the amounts used to prepare the electrolytes for 1000 ml

Reagents	Electrolyte 1	Electrolyte 2	Electrolyte 3
$\text{Ca}(\text{C}_2\text{H}_3\text{O}_2)_2 \cdot \text{H}_2\text{O}$	0.06 M	0.06 M	0.06 M
$\text{Na}_3\text{PO}_4 \cdot 12\text{H}_2\text{O}$	0.01 M	0.01 M	0.01 M
$\text{Na}_2\text{B}_4\text{O}_7 \cdot 10\text{H}_2\text{O}$	0.005 M	0.01 M	-

2.2. Method

An AC-pulsed power supply was used in the bipolar mode for plasma electrolytic oxidation. The PEO process was carried out in an electrolytic cell where the stainless-steel bath was used as a counter electrode and the samples served as the anode. The electrolytes were stirred continuously with a stirring speed of 250 rpm. The temperature of the electrolytes was kept constant during the experiments via a circulation pump. Table 2 shows the PEO process parameters that were determined based on past research (Vangolu & Kilic, 2022).

Table 2. PEO process parameters

Process	Frequency (Hz)	Duty cycle (%)	Voltage (V)	Time (min)	Solution stirring speed (rpm)
PEO	300	10	+500 / -100	5	250

2.3. Analysis

2.3.1. Coatings characterisations

Carl Zeiss Sigma 300 scanning electron microscope (SEM) equipped with energy dispersive spectroscopy (EDS) was utilised to analyse and characterise the surface. An incident beam energy of 20 kV was used for both SEM and EDS. A Panalytical Empyrean X-ray diffractometer (XRD) with $\text{CuK}\alpha$ ($\lambda = 1.5406 \text{ \AA}$) radiation at 45 kV and 40 mA was used in continuous scan mode for the phase analyses. The conventional Bragg-Brentano XRD technique was used in analyses. The measurements were performed from the substrate to the outer layer via distance. The surface roughness of the specimens was evaluated using a MAHR perthometer.

2.3.2. Static corrosion experiments

All electrochemical experiments were performed using a Gamry G750 potentiostat/galvanostat apparatus and a standard three-electrode cell with a platinum electrode as the counter electrode, a saturated Ag/AgCl electrode as the reference electrode, and the samples as the working electrode. The contact area of the samples with the electrolyte was 0.38 cm^2 and the experiments were started after they were immersed in the electrolyte for 7200 seconds to reach the steady state OCP value. The potential data were recorded as a function of time during immersion. The forward scan of the cyclic potentiodynamic polarization studies was performed in the range of -250 mV (vs. OCP) to $+2000 \text{ mV}$ with a scan rate of 1 mV/s . The backward scan was performed from peak to OCP at the same scan rate. The electrochemical impedance spectra were recorded in a frequency range from 10 kHz to 10 MHz . In order to see the effect of polarization experiments on the surface, impedance analysis was performed both before and after polarization. EIS spectra were fitted to experimental data obtained using a suitable equivalent electrical circuit representing the surface conditions. The results are presented normalized by area for comparability with the scientific literature as much as possible. The electrolyte used in corrosion tests was a 25% (v/v) foetal bovine serum (FBS) prepared according to ISO 14242-1 standard. The FBS was diluted by adding phosphate buffer solution (PBS) in order to reach a total protein content which is close to the conditions *in vivo*. Also, sodium azide was added to the solution to retard bacterial growth. For the simulation of inflammatory conditions *in vivo*, hydrogen peroxide (H_2O_2) was supplemented into the serum.

3. Results and discussion

3.1. Structural characterisation

Figure 1 depicts the XRD patterns of the untreated, E1, E2, and E3 samples. Because Ti45Nb is a β titanium alloy, all β -Ti peaks were seen in the patterns as expected. The two primary polymorphs of TiO_2 , rutile and anatase, were found in all treated samples after the oxidation procedure. The rutile and anatase phases were identified using JCPDS 01-087-0710 and JCPDS 01-086-1764 cards, respectively. Despite the fact that the intensity of boron was not noticed in the XRD pictures of the E1 and E2 samples, the scientific literature indicates that it exists in the amorphous TiO_2 layer and sometimes causes a shoulder between $25^\circ - 30^\circ$. Actually, an increase was observed in the rutile phase peaks as the amount of boron in the electrolyte increased. Especially, the rutile peak at 27° increased significantly with increasing boron content. When the XRD graph is examined, decreases in the densities of the peaks achieved from the substrate are observed in the samples subjected to PEO treatment in the boron-containing electrolyte. It can be said that the presence of boron in the structure causes the densities of the peaks measured from the base material to decrease.

Figure 2 shows the surface topography and the EDS analyses of the coated samples. It can be seen from Figure 2 (a, b and c) that the highly porous and rough oxide layer, which are two of the main features of the process, is formed on all surfaces after PEO. The roughness of the layers was measured as 1.693 ± 0.02 , 1.676 ± 0.02 and 1.712 ± 0.02 for E1, E2 and E3 samples respectively. The pores of different dimensions including micro and sub-micro pores, which can mainly be related to frequency and voltage, are homogeneously dispersed over the entire surface. It is known that PEO allows adjusting the pore size and roughness by changing process parameters like voltage, frequency and time (Huang et al., 2005; Wang et al., 2010). Besides a study by Lv et al. (2008) indicated that larger pore diameters and rougher film layers can be obtained with coatings made at lower frequencies. It is obvious that the boron addition (Figure 2a and Figure 2b) had no notable effect on the SEM images of the coated layer.

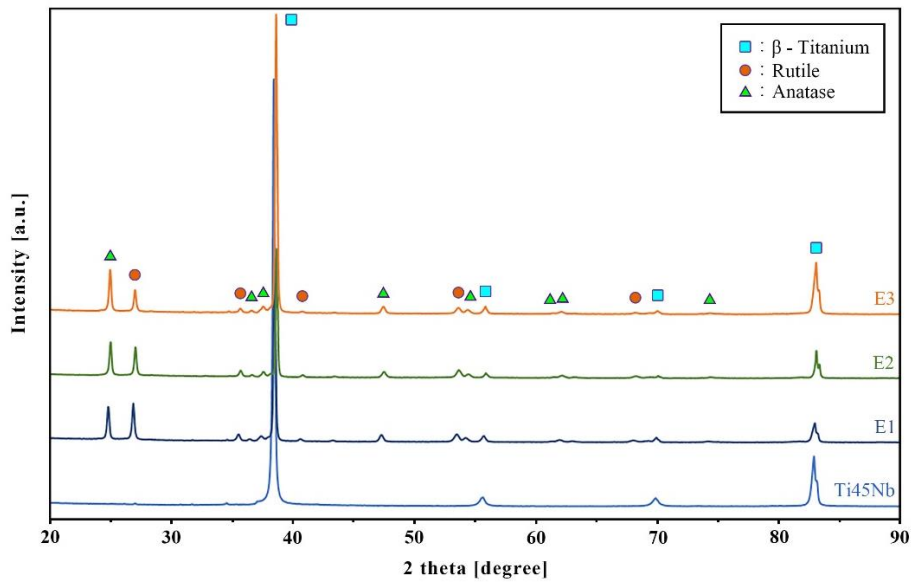


Figure 1. The XRD graphics of untreated, E1, E2, and E3 samples

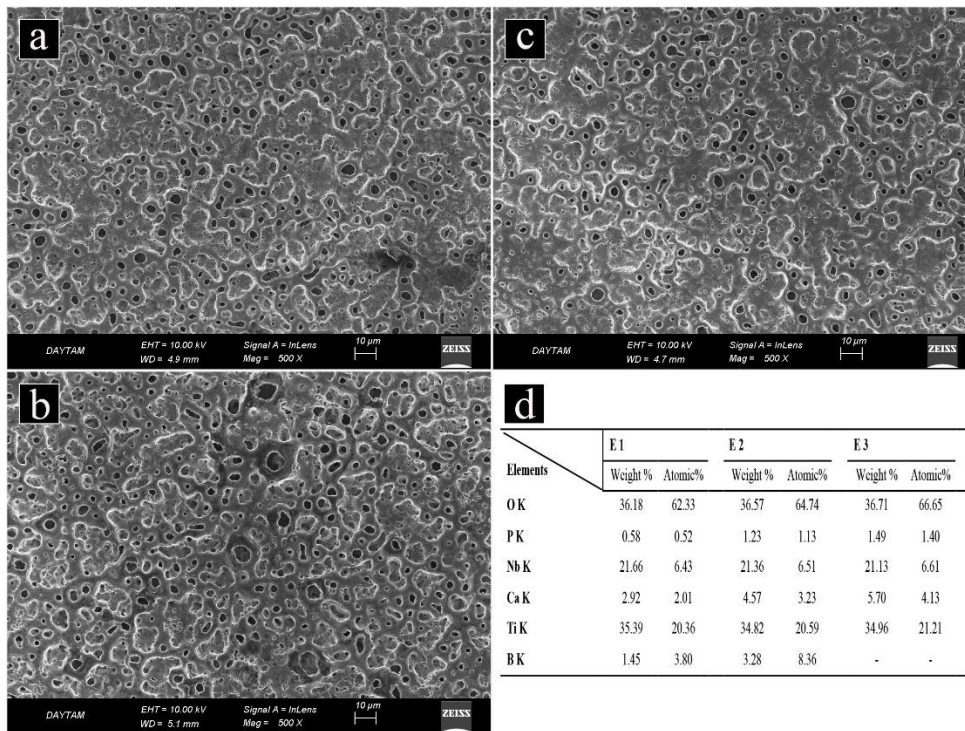


Figure 2. The SEM micrographs of a) E1, b) E2, c) E3 and the EDS results of d) all samples

Although there was no clear peak in XRD analyses regarding the presence of boron in the structure, EDS analyses show that there are certain amounts of boron inside the structure of E1 and E2 samples with atomic ratios of 3.80% and 8.36%, respectively (Figure 2d). According to a scientific study, by optimizing the accelerating voltage boron can be analysed by EDS (Ingemarsson & Halvarsson, 2011). Similarly, Ca and P elements, which are the basis of the electrolytes in this study, were also identified in EDS analyses as expected.

3.2. Corrosion tests

Figure 3 shows the changes in the open circuit potential of the samples in serum. All surface-treated samples had a higher potential than the untreated sample. Under E2 and E3 conditions, the potential values decreased

slightly from the initial values and stabilized, indicating that the activity of the samples increased due to contact with the electrolyte. All treated samples have approximately equal equilibrium potentials.

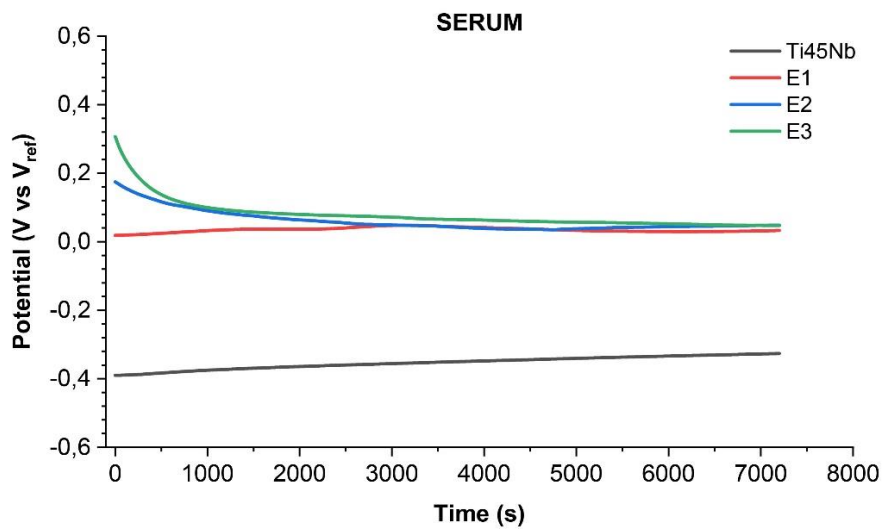


Figure 3. The changes in the open circuit potential of the samples in serum

Open circuit potentials of samples in Serum+H₂O₂ solution are given in Figure 4. In the serum medium to which H₂O₂ was added, the samples exhibited more stable curves. On the other hand, in contrast to the pure serum medium, the treated samples had different values and the equilibrium potential was slightly higher for all samples. Sample E2 had the most inert value.

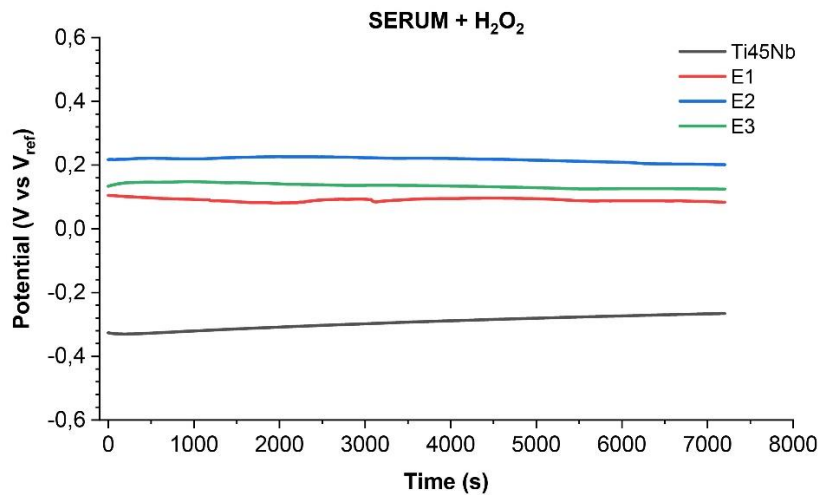


Figure 4. Open circuit potentials of samples in serum+H₂O₂ solution

Cyclic polarization curves in Serum can be seen in Figure 5 and corrosion parameters obtained by Tafel extrapolation are given in Table 3. Although it is noted that the corrosion current density and therefore the corrosion rate of the untreated sample is higher than the other samples, it can be seen that it shows passivation behaviour in the range of approximately 10 mV to 1400 mV, but this behaviour is not a complete passivation due to the slow increase in current density.

As can be seen from Table 3, the beta values of the anodic branch (Beta A) in the curves of the treated specimens were generally quite high. This could be interpreted as diffusion-controlled corrosion. That is, the diffusion of electrochemically active species to the surface was limited due to the surface roughness or, in other words, the stagnation of the solution in the pores. However, no passivation behaviour was observed in the treated samples. Active dissolution continued steadily throughout the experiment, with E2 being slower and E1 being faster. In the reverse scanning curves, the anode-cathode transition was also detected again due to the increase of the open circuit potential due to polarization.

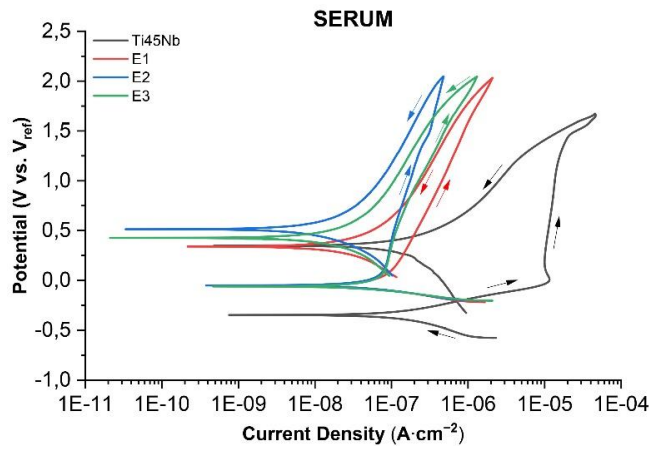


Figure 5. Cyclic polarization curves in serum

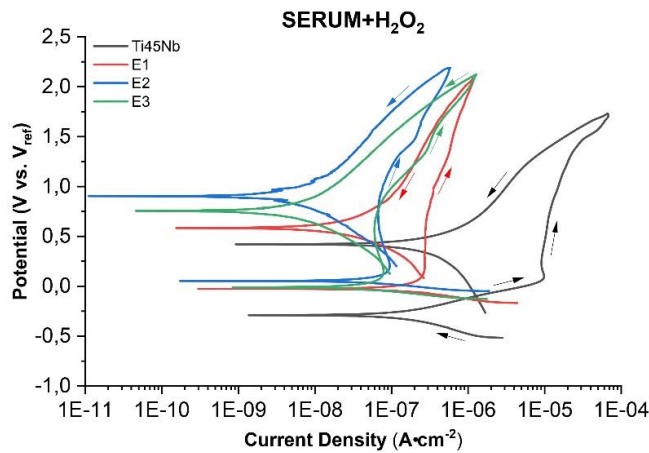


Figure 6. Cyclic polarization curves in H₂O₂-added Serum

Figure 6 shows the cyclic polarization curves in H₂O₂-added serum and Table 3 shows the values obtained by Tafel extrapolation. The untreated sample had an overall higher current density. It exhibited a passivity-like behaviour in the range from 0 to 1500 mV, followed by a trans-passive region. The Tafel regions of the untreated samples were close to each other, and the anodic and cathodic arms were neighbouring. A passive region of approximately 1000 mV was detected in all conditions. This was more pronounced in E2 and E3 conditions. In condition E1, the active dissolution rate after passivity was slightly slower than the others. Anodic beta values were very high in all treated conditions, indicating a diffusion-controlled mechanism.

In none of the samples did the reverse scanning curve intersect the forward scanning curve. Therefore, it could be said that general surface corrosion was present rather than localized corrosion.

Table 3. Tafel coefficients and corrosion parameters

SERUM								
	Ti45Nb		E1		E2		E3	
	Mean	SD	Mean	SD	Mean	SD	Mean	SD
Beta A (V/decade)	2.26E-01	6.99E-03	2.13E+00	4.47E-01	1.00E+15	0.00E+00	9.06E+00	2.90E+00
Beta C (V/decade)	2.68E-01	2.90E-03	1.71E-01	3.48E-03	1.55E-01	3.09E-04	1.39E-01	9.44E-04
I_{corr} (A·cm⁻²)	1.77E-07	3.86E-09	9.33E-08	3.35E-09	8.84E-08	3.09E-10	8.38E-08	1.02E-09
E_{corr} (mV)	-3.47E+02	0.00E+00	-5.09E+01	0.00E+00	-5.05E+01	0.00E+00	-6.00E+01	0.00E+00
Cor. rate (mpy)	5.58E-02	1.29E-03	2.94E-02	1.96E-03	2.78E-02	1.05E-03	2.64E-02	1.26E-03

Table 3. continues.

SERUM + H ₂ O ₂								
	Ti45Nb		E1		E2		E3	
	Mean	SD	Mean	SD	Mean	SD	Mean	SD
Beta A (V/decade)	2.57E-01	1.13E-02	6.67E+14	4.71E+14	1.00E+15	0.00E+00	1.00E+15	0.00E+00
Beta C (V/decade)	2.54E-01	1.23E-02	1.51E-01	6.50E-03	1.21E-01	2.32E-03	1.25E-01	1.50E-03
I_{corr} (A·cm⁻²)	2.00E-07	9.42E-09	2.92E-07	2.25E-08	1.09E-07	2.16E-09	8.97E-08	5.00E-11
E_{corr} (mV)	-2.89E+02	0.00E+00	-2.61E+01	3.55E-15	5.33E+01	7.11E-15	-1.06E+01	0.00E+00
Cor. rate (mpy)	6.30E-02	2.96E-03	7.19E-02	7.10E-03	3.43E-02	1.69E-03	2.82E-02	1.12E-03

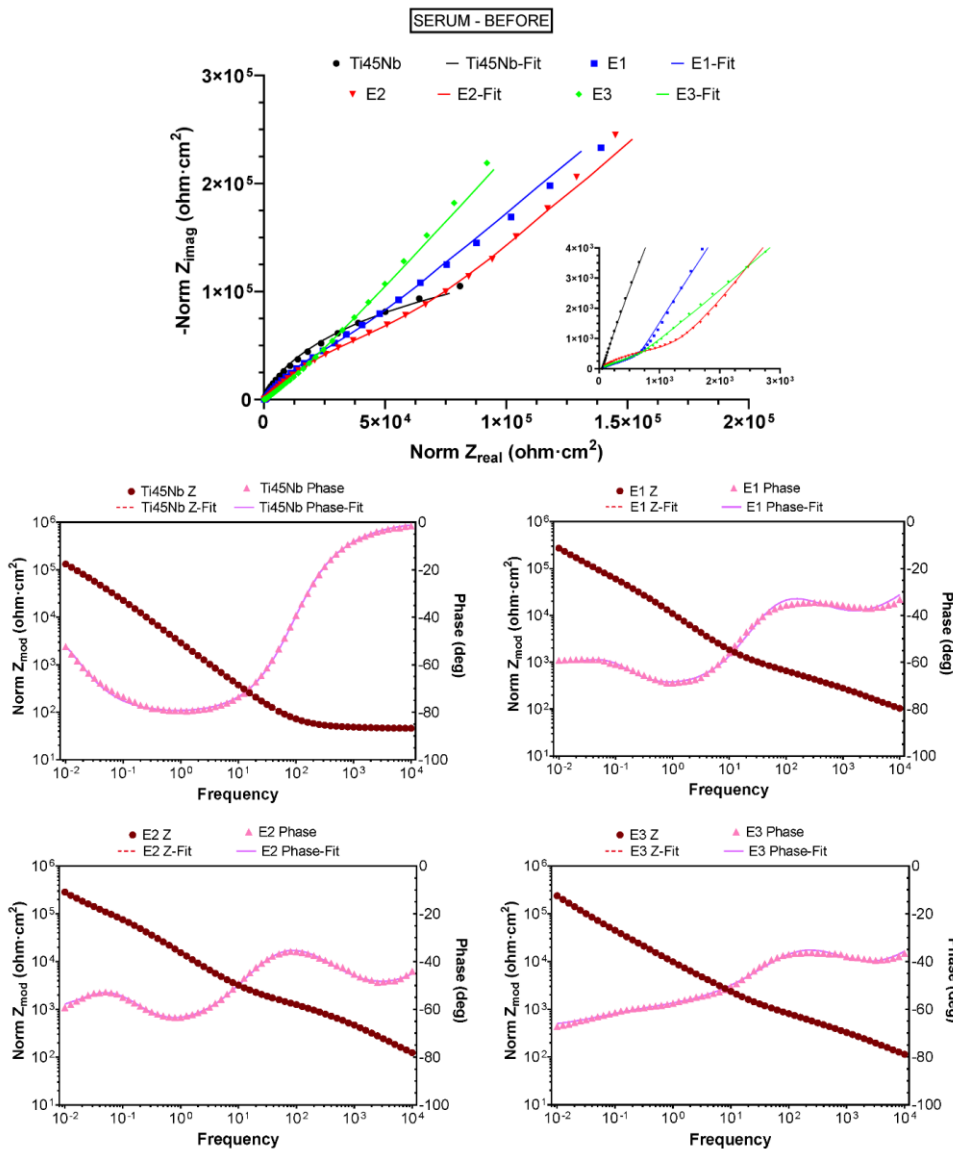
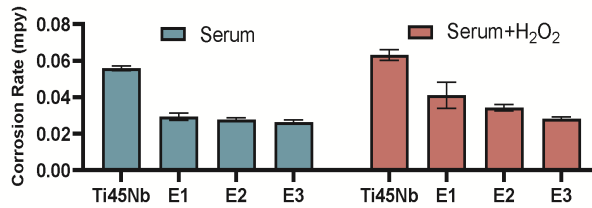


Figure 7. Results obtained from EIS experiments performed on treated and untreated Ti45Nb alloy specimens in serum

Results obtained from EIS experiments performed on treated and untreated Ti45Nb alloy specimens in serum are given in Figure 7. As seen in the Bode diagram, the EIS responses of the coatings E1 and E2 showed two distinct time constants, which can be interpreted as the formation of an oxide film consisting of two layers. The first time constant at low frequencies may be associated with a dense and continuous layer in contact with the metal surface, known as the inner layer, and the second time constant (at high frequencies) may be associated with the porous outer layer, formed by the dielectric breakdown of the insulating film. On the other hand, in the case of E3, the second time constant was still present but not very pronounced. It is also noteworthy that while the phase angle of the untreated sample approaches zero at high frequencies, it is around 40 degrees in the surface-treated samples. In addition, the Nyquist diagram showed a linear portion with about 45° angle indicating a diffusion process.

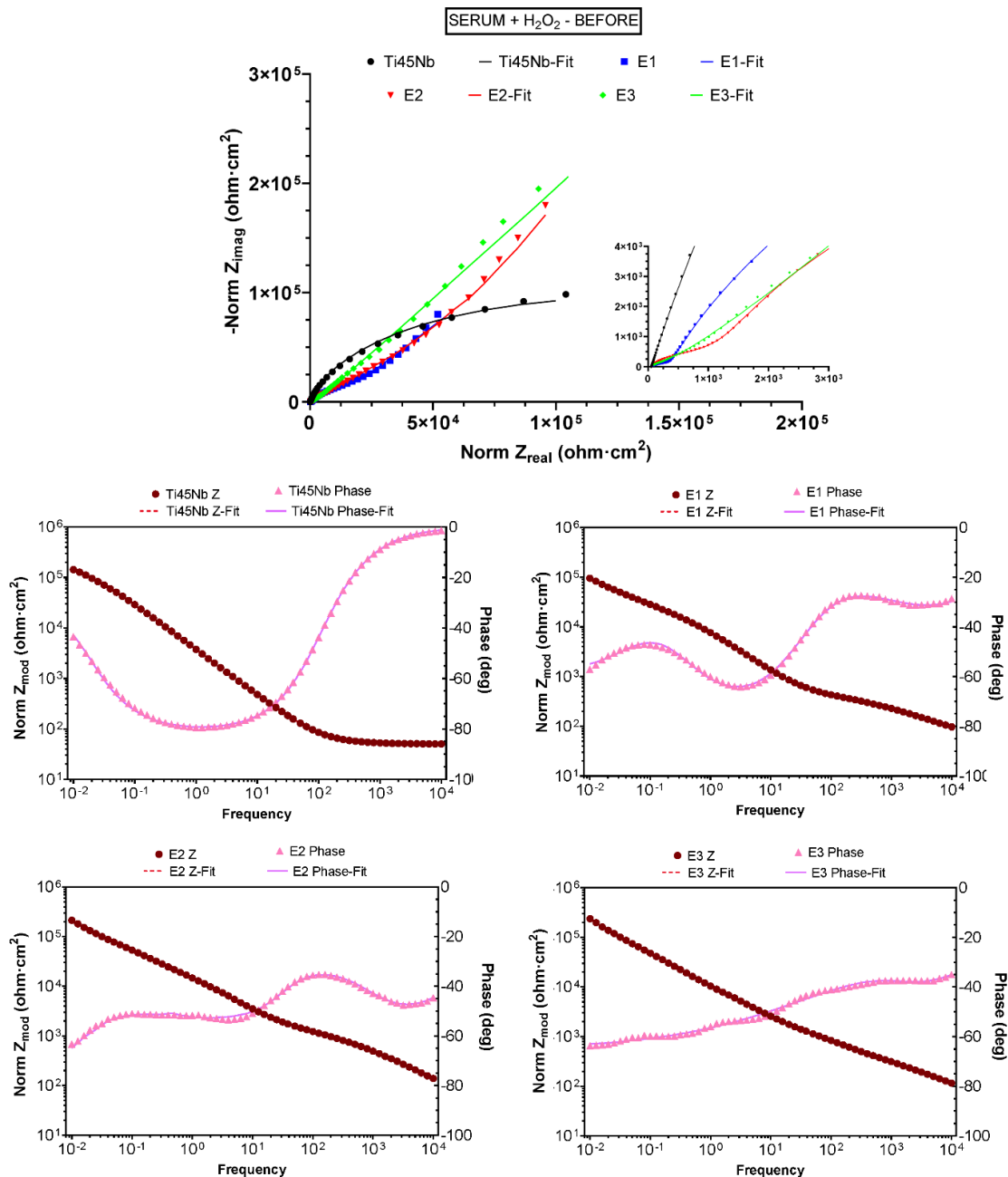


Figure 8. The EIS results of treated and untreated Ti45Nb samples in Serum+H₂O₂ electrolyte.

Figure 8 shows the EIS results of treated and untreated Ti45Nb samples in Serum+H₂O₂ electrolyte. The untreated sample showed almost identical behaviour in this solution as in the serum. The two time constants were again visible in samples E1 and E2, while sample E3 exhibited a pseudo-linear curve. However, on closer inspection, time constants could still be observed and even a third one can be argued.

An electrical equivalent circuit model was created using the experimental results of the EIS tests and given in Figure 9. The proposed model consisted of resistance elements for the solution (R_{sol}), porous layer (R_{po}) and barrier layer (R_{ba}) and constant phase elements (CPE) for the porous (C_{po}) and barrier (C_{ba}) layers. Furthermore, a phase element (C_{di}) was added in series with R_{ba} to represent the diffusion of ions. A Warburg impedance could be utilized for the same goal, but it would further complicate the model. A similar equivalent circuit has been proposed by other studies. For both electrolytes, the fit curves given in the Nyquist and Bode plots of all samples show that the simulated data obtained by this model are in good agreement with the experimental results. The EIS parameters of surface layers are summarized in Table 4.

Table 4. Electrochemical impedance parameters of surface layers on pure untreated and oxidized Ti45Nb alloy

SERUM								
	Ti45Nb		E1		E2		E3	
	Mean	SD	Mean	SD	Mean	SD	Mean	SD
R_{sol} ($\Omega \cdot cm^{-2}$)	46.11	9.02E-01	46.91	3.74E-01	45.77	6.32E-01	46.13	6.98E-01
R_{po} ($\Omega \cdot cm^{-2}$)	4.37	1.07	922.8	56.5	1686.1	129	477.9	12.8
C_{po} ($S \cdot s^a \cdot cm^{-2}$)	4.90E-05	2.60E-06	1.44E-05	2.14E-06	5.44E-06	1.08E-07	9.64E-06	4.80E-07
m	1.00	6.64E-02	6.24E-01	1.64E-02	6.73E-01	2.12E-02	6.78E-01	5.13E-02
R_{ba} ($\Omega \cdot cm^{-2}$)	1.43E+04	1.12E+03	1.49E+04	9.81E+03	3.40E+04	7.83E+03	1.48E+04	1.55E+03
C_{ba} ($S \cdot s^a \cdot cm^{-2}$)	8.20E-05	5.53E-06	8.93E-05	3.53E-06	3.81E-05	4.11E-06	9.12E-05	3.73E-06
n	8.93E-01	7.43E-02	1.00	1.44E-02	9.15E-01	6.11E-02	5.35E-01	3.46E-02
C_{di} ($S \cdot s^a \cdot cm^{-2}$)	2.90E-04	9.11E-05	1.43E-05	4.71E-06	2.13E-05	1.56E-06	2.73E-05	5.81E-06
k	9.14E-01	5.86E-02	8.42E-01	3.12E-02	7.18E-01	2.27E-02	8.03E-01	8.06E-02
SERUM + H₂O₂								
	Ti45Nb		E1		E2		E3	
	Mean	SD	Mean	SD	Mean	SD	Mean	SD
R_{sol} ($\Omega \cdot cm^{-2}$)	35.27	6.98E-01	34.73	6.26E-01	34.55	7.15E-01	36.89	70.08E-01
R_{po} ($\Omega \cdot cm^{-2}$)	5.57	0.86	416.6	42.17	5074	226	112.1	26
C_{po} ($S \cdot s^a \cdot cm^{-2}$)	2.59E-04	5.95E-05	2.72E-05	6.84E-06	2.38E-05	7.63E-07	2.64E-05	1.78E-06
m	8.88E-01	4.69E-02	5.58E-01	2.76E-02	5.73E-01	9.84E-03	9.24E-01	9.58E-02
R_{ba} ($\Omega \cdot cm^{-2}$)	1.55E+05	1.15E+03	1.56E+04	6.71E+02	375.2	26.3	2.85E+04	6.31E+02
C_{ba} ($S \cdot s^a \cdot cm^{-2}$)	5.75E-05	3.46E-06	4.05E-05	9.29E-06	3.01E-06	1.03E-06	2.59E-04	1.11E-04
n	8.95E-01	8.32E-02	8.38E-01	7.44E-02	8.03E-01	5.26E-02	3.84E-01	2.35E-02
C_{di} ($S \cdot s^a \cdot cm^{-2}$)	1.96E-04	1.54E-05	5.81E-05	1.88E-06	8.22E-07	6.77E-08	3.13E-05	1.99E-06
k	1.00	1.41E-02	8.41E-01	1.72E-02	1.00	1.18E-01	7.15E-01	1.26E-02

Since the natural layer on the surface of the untreated sample is very thin and non-porous, the R_{po} resistance is low in both electrolytes. It was mentioned earlier that the PEO treatment makes the surface porous, thus increasing the R_{po} resistance. The highest value was observed at the E2 condition for both electrolytes. Regarding the barrier layer, the situation seems to be reversed. The untreated conditions show higher values compared to the oxidized samples. It can be concluded that during oxidation the surface layer thickens and becomes porous. In some conditions, the CPE exponents were seen to approach very close to or reach the value of 1. This indicates that the element behaves in a similar way to an ideal capacitor under these conditions.

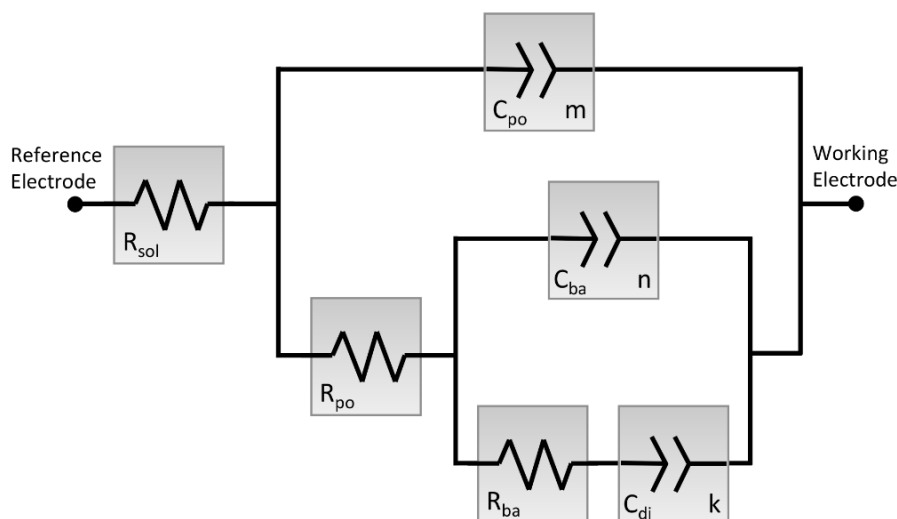


Figure 9. Electrical equivalent circuit model

4. Conclusions

In this study, a boron, calcium and phosphate doped oxide layer was successfully formed on the Ti45Nb surface using the PEO method according to the EDS results. The effect of boron amount in the electrolyte on surface properties and corrosion resistance was investigated. After PEO a rough and porous oxide layer, which is beneficial for the bone-growth and rapid osseointegration, was observed on the surface. Pores with different sizes were homogeneously distributed all over the surface. Except for the decrease in the number of pores observed in some regions, no effect of boron embedding was observed in terms of surface SEM views.

It can be said that the surface treatment increased the corrosion resistance. Especially the boron embedded samples exhibited better corrosion properties as they were found to be relatively more noble. The corrosion mechanisms of the treated samples were thought to be diffusion-controlled corrosion as the Beta A values were found to be quite high. The treated samples didn't show a passivation behaviour. According to Tafel extrapolation, the current density was higher in the untreated sample. General surface corrosion was observed as the reverse scanning curve didn't intersect the forward scanning curve in any of the samples.

E1 and E2, both boron-doped samples, had the best corrosion resistance. Boron-doped, CaP-containing TiO₂ layers coated with PEO could be a promising option for improving the bioactivity and biocompatibility of Ti45Nb biomaterials, as well as bone-tissue healing, anti-bacterial, and anti-inflammatory capabilities.

Acknowledgement

The authors would like to thank Atatürk University East Anatolia High Technology Application and Research Center (DAYTAM) and Erzurum Technical University High Technology Application and Research Center (YUTAM) for their assistance during the characterization of specimens.

Author contribution

S. Yenal Vangölü; conceived and designed the analysis, collected the data, contributed data or analysis tools, performed the analysis and wrote the paper.

Özgü Bayrak; conceived and designed the analysis, contributed data or analysis tools, performed the analysis and wrote the paper.

Declaration of ethical code

In this study, we undertake that all the rules that must be followed within the scope of the "Higher Education Institutions Scientific Research and Publication Ethics Directive" have been complied with and that none of

the actions specified under the heading "Actions Contrary to Scientific Research and Publication Ethics" have been carried out in the said directive."

The authors of this article declare that the materials and methods used in this study do not require ethical committee approval and/or legal-specific permission."

Conflicts of interest

The authors declare that they have no known competing financial interests or personal relationships that could have appeared to influence the work reported in this paper.

References

- Atila, A., Halici, Z., Cadirci, E., Karakus, E., Palabiyik, S. S., Ay, N., Bakan, F., & Yilmaz, S. (2016). Study of the boron levels in serum after implantation of different ratios nano-hexagonal boron nitride-hydroxy apatite in rat femurs. *Materials Science and Engineering C*, *58*, 1082–1089. <https://doi.org/10.1016/j.msec.2015.09.041>
- Bai, Y., Deng, Y., Zheng, Y., Li, Y., Zhang, R., Lv, Y., Zhao, Q., & Wei, S. (2016). Characterization, corrosion behavior, cellular response and in vivo bone tissue compatibility of titanium–niobium alloy with low Young's modulus. *Materials Science and Engineering: C*, *59*, 565–576. <https://doi.org/10.1016/J.MSEC.2015.10.062>
- Chen, Q., & Thouas, G. (2014). *Biomaterials: A basic introduction* (1st ed.). CRC Press. <https://doi.org/10.1201/b17553>
- Cheng, J., Peng, K., Jin, E., Zhang, Y., Liu, Y., Zhang, N., Song, H., Liu, H., & Tang, Z. (2011). Effect of additional boron on tibias of African ostrich chicks. *Biological Trace Element Research*, *144*(1–3), 538–549. <https://doi.org/10.1007/s12011-011-9024-y>
- Elias, C. N., Lima, J. H. C., Valiev, R., & Meyers, M. A. (2008). Biomedical applications of titanium and its alloys. *JOM*, *60*(3), 46–49. <https://doi.org/10.1007/S11837-008-0031-1>
- Esfahani, E. A., Bukuaghangin, O., Banfield, S., Vangözü, Y., Yang, L., Neville, A., Hall, R., & Bryant, M. (2022). Surface engineering of wrought and additive layer manufactured Ti-6Al-4V alloy for enhanced load bearing and bio-tribocorrosion applications. *Surface and Coatings Technology*, *442*, 128139. <https://doi.org/10.1016/J.SURFCOAT.2022.128139>
- Gebert, A., Eigel, D., Gostin, P. F., Hoffmann, V., Uhlemann, M., Helth, A., Pilz, S., Schmidt, R., Calin, M., Göttlicher, M., Rohnke, M., & Janek, J. (2016). Oxidation treatments of beta-type Ti-40Nb for biomedical use. *Surface and Coatings Technology*, *302*, 88–99. <https://doi.org/10.1016/J.SURFCOAT.2016.05.036>
- Hakki, S. S., Bozkurt, B. S., & Hakki, E. E. (2010). Boron regulates mineralized tissue-associated proteins in osteoblasts (MC3T3-E1). *Journal of Trace Elements in Medicine and Biology*, *24*(4), 243–250. <https://doi.org/10.1016/j.jtemb.2010.03.003>
- Huang, P., Xu, K. W., & Han, Y. (2005). Preparation and apatite layer formation of plasma electrolytic oxidation film on titanium for biomedical application. *Materials Letters*, *59*(2–3), 185–189. <https://doi.org/10.1016/j.matlet.2004.09.045>
- Ingemarsson, L., & Halvarsson, M. (2011). *SEM / EDX analysis of boron 2011-0131 a case study*. Chalmers University of Technology. http://fy.chalmers.se/~f10mh/Halvarsson/EM_intro_course_files/SEM_EDX%20Boron.pdf
- Johansson, C. B., & Albrektsson, T. (1991). A removal torque and histomorphometric study of commercially pure niobium and titanium implants in rabbit bone. *Clinical Oral Implants Research*, *2*(1), 24–29. <https://doi.org/10.1034/J.1600-0501.1991.020103.X>
- Long, M., & Rack, H. J. (1998). Titanium alloys in total joint replacement—a materials science perspective. *Biomaterials*, *19*(18), 1621–1639. [https://doi.org/10.1016/S0142-9612\(97\)00146-4](https://doi.org/10.1016/S0142-9612(97)00146-4)
- Lv, G. H., Chen, H., Gu, W. C., Li, L., Niu, E. W., Zhang, X. H., & Yang, S. Z. (2008). Effects of current frequency on the structural characteristics and corrosion property of ceramic coatings formed on magnesium alloy by PEO technology. *Journal of Materials Processing Technology*, *208*(1–3), 9–13. <https://doi.org/10.1016/j.jmatprotec.2007.12.125>

- Matsuno, H., Yokoyama, A., Watari, F., Uo, M., & Kawasaki, T. (2001). Biocompatibility and osteogenesis of refractory metal implants, titanium, hafnium, niobium, tantalum and rhenium. *Biomaterials*, 22(11), 1253–1262. [https://doi.org/10.1016/S0142-9612\(00\)00275-1](https://doi.org/10.1016/S0142-9612(00)00275-1)
- Niinomi, M. (2003). Recent research and development in titanium alloys for biomedical applications and healthcare goods. *Science and Technology of Advanced Materials*, 4(5), 445–454. <https://doi.org/10.1016/J.STAM.2003.09.002>
- Niinomi, M., & Boehlert, C. J. (2015). Titanium alloys for biomedical applications. In M. Niinomi, T. Narushima, & M. Nakai (Eds.), *Advances in Metallic Materials* (ss. 179–213). Springer. https://doi.org/10.1007/978-3-662-46836-4_8
- Ozaki, T., Matsumoto, H., Watanabe, S., & Hanada, S. (2004). Beta Ti alloys with low Young's modulus. *Materials Transactions*, 45(8), 2776–2779. <https://doi.org/10.2320/MATERTRANS.45.2776>
- Sopchenski, L., Cogo, S., Dias-Ntipanyj, M. F., Elifio-Espósito, S., Popat, K. C., & Soares, P. (2018). Bioactive and antibacterial boron doped TiO₂ coating obtained by PEO. *Applied Surface Science*, 458, 49–58. <https://doi.org/10.1016/j.apsusc.2018.07.049>
- Taşlı, P. N., Yalvaç, M. E., Sofiev, N., & Şahin, F. (2013). Effect of F68, F127, and P85 pluronic block copolymers on odontogenic differentiation of human tooth germ stem cells. *Journal of Endodontics*, 39(10), 1265–1271. <https://doi.org/10.1016/j.joen.2013.06.011>
- Valiev, R. Z., Estrin, Y., Horita, Z., Langdon, T. G., Zehetbauer, M. J., & Zhu, Y. T. (2015). Fundamentals of superior properties in bulk NanoSPD materials. *Materials Research Letters*, 4(1), 1–21. <https://doi.org/10.1080/21663831.2015.1060543>
- Vangolu, Y., & Kilic, S. (2022). Corrosion and wear performances of hydroxyapatite and boron-containing TiO₂ composite coatings on Ti6Al7Nb alloy. *Surface Topography: Metrology and Properties*, 10(2), 025030. <https://doi.org/10.1088/2051-672X/AC7816>
- Wang, Y., Wang, L., Zheng, H., Du, C., ChengyunNing, Shi, Z., & Xu, C. (2010). Effect of frequency on the structure and cell response of Ca- and P-containing MAO films. *Applied Surface Science*, 256(7), 2018–2024. <https://doi.org/10.1016/j.apsusc.2009.09.041>
- Yavari, S. A., Necula, B. S., Fratila-Apachitei, L. E., Duszczuk, J., & Apachitei, I. (2016). Biofunctional surfaces by plasma electrolytic oxidation on titanium biomedical alloys. *Surface Engineering*, 32(6), 411–417. <https://doi.org/10.1179/1743294415Y.0000000101>
- Ying, X., Cheng, S., Wang, W., Lin, Z., Chen, Q., Zhang, W., Kou, D., Shen, Y., Cheng, X., Rompis, F. A., Peng, L., & Lu, C. Z. (2011). Effect of boron on osteogenic differentiation of human bone marrow stromal cells. *Biological Trace Element Research*, 144(1–3), 306–315. <https://doi.org/10.1007/s12011-011-9094-x>